# Tunable ring laser with internal injection seeding and an optically-driven photonic crystal reflector

**Jie Zheng,[1] Chun Ge,[1]Clark J. Wagner,[1] Meng Lu,[2] Brian T. Cunningham,[1,3] J. Darby Hewitt,[1,*]and J. Gary Eden[1]**

[1]*Department of Electrical and Computer Engineering, University of Illinois, Urbana, Illinois 61801, USA*
[2]*SRU Biosystems, 14-A Gill Street, Woburn, Massachusetts 01810, USA*
[3]*Department of Bioengineering, University of Illinois, Urbana, Illinois 61801, USA*
[*]*hewitt3@illinois.edu*

**Abstract:** Continuous tuning over a 1.6 THz region in the near-infrared (842.5-848.6 nm) has been achieved with a hybrid ring/external cavity laser having a single, optically-driven grating reflector and gain provided by an injection-seeded semiconductor amplifier. Driven at 532 nm and incorporating a photonic crystal with an azobenzene overlayer, the reflector has a peak reflectivity of ~80% and tunes at the rate of 0.024 nm per mW of incident green power. In a departure from conventional ring or external cavity lasers, the frequency selectivity for this system is provided by the passband of the tunable photonic crystal reflector and line narrowing in a high gain amplifier. Sub - 0.1 nm linewidths and amplifier extraction efficiencies above 97% are observed with the reflector tuned to 842.5 nm.



**OCIS codes:** (050.5298) Photonic crystals; (140.3520) Lasers, injection-locked; (140.3560) Lasers, ring; (140.3480) Lasers, diode-pumped.

## References and links

1. J. W. Crowe and R. M. Craig, Jr., "GaAs laser linewidth measurements by heterodyne detection," Appl. Phys. Lett. **5**(4), 72–74 (1964).
2. R. Ludeke and E. P. Harris, "Tunable GaAs laser in an external dispersive cavity," Appl. Phys. Lett. **20**(12), 499–500 (1972).
3. B. Mroziewicz, "External cavity wavelength tunable semiconductor lasers—a review," Opto-Electron. Rev. **16**(4), 347–366 (2008).
4. A. S. P. Chang, H. Tan, S. Bai, W. Wu, Z. Yu, and S. Y. Chou, "Tunable external cavity laser with a liquid-crystal subwavelength resonant grating filter as wavelength-selective mirror," IEEE Photon. Technol. Lett. **19**(14), 1099–1101 (2007).
5. D. W. Dobbs and B. T. Cunningham, "Optically tunable guided-mode resonance filter," Appl. Opt. **45**(28), 7286–7293 (2006).
6. C. Ge, M. Lu, X. Jian, Y. Tan, and B. T. Cunningham, "Large-area organic distributed feedback laser fabricated by nanoreplica molding and horizontal dipping," Opt. Express **18**(12), 12980–12991 (2010).
7. J. Zheng, J. Y. Kim, S. K. Lee, S.-J. Park, and J. G. Eden, "Molded arrays of microcavities and channels in polymer structures: ultraviolet emitting microplasma sources for biophotonics," IEEE Trans. Plasma Sci. **36**(4), 1256–1257 (2008).
8. M. Ivanov, D. Ilieva, G. Minchev, T. Petrova, V. Dragostinova, T. Todorov, and L. Nikolova, "Temperature-dependent light intensity controlled optical switching in azobenzene polymers," Appl. Phys. Lett. **86**(18), 181902 (2005).
9. L. L. Nedelchev, A. S. Matharu, S. Hvilsted, and P. S. Ramanujam, "Photoinduced anisotropy in a family of amorphous azobenzene polyesters for optical storage," Appl. Opt. **42**(29), 5918–5927 (2003).
10. V. Bolpasi and W. von Klitzing, "Double-pass tapered amplifier diode laser with an output power of 1 W for an injection power of only 200 μW," Rev. Sci. Instrum. **81**(11), 113108 (2010).
11. L. W. Casperson and A. Yariv, "Spectral narrowing in high-gain lasers," IEEE J. Quantum Electron. **8**(2), 80–85 (1972).
12. G. Smith, P. C. Shardlow, and M. J. Damzen, "High-power near-diffraction-limited solid-state amplified spontaneous emission laser devices," Opt. Lett. **32**(13), 1911–1913 (2007).
13. A. E. Siegman, *Lasers* (University Science Books, 1986), pp. 547–557.

#158009 - $15.00 USD Received 21 Nov 2011; revised 1 Feb 2012; accepted 5 Jun 2012; published 12 Jun 2012

14. J. Goldhar and J. R. Murray, "Injection-locked, narrow-band KrF discharge laser using an unstable resonator cavity," Opt. Lett. **1**(6), 199–201 (1977).
15. D. P. Greene and J. G. Eden, "Injection locking and saturation intensity of a cadmium iodide laser," Opt. Lett. **10**(2), 59–61 (1985).

## 1. Introduction

Since their introduction in 1964 (Ref. 1) and the demonstration of tunable systems eight years later [2], external cavity lasers [3] have had an enormous impact on spectroscopy and applications such as chemical diagnostics and atom traps. Despite offering single-mode, continuous wave (cw) output from a generally compact package, however, external cavity lasers (ECLs) that are tunable invariably require the physical movement of at least one optic [3]. Because a mechanical rotation or translation stage is necessary to rotate a grating or prism, stretch a fiber Bragg grating, or vary the cavity length of an etalon, such lasers are often unduly bulky, as well as complex to assemble and operate. One notable exception is the recent report [4] of an ECL employing, as the frequency-selective optic, a liquid crystal filter with a reflectivity ≤ 60%.

In this article, a tunable external cavity laser in an injection-seeded ring configuration incorporating a resonant reflector driven by an external optical source is described. Filtering the amplified spontaneous emission (ASE) from a semiconductor amplifier with a photonic crystal reflector yields a master oscillator-power amplifier (MOPA) system for which the efficiency for extracting, in a narrow bandwidth (< 0.1 nm) line, the power radiated by the amplifier is as high as > 97%. Tuning the reflector over a wavelength interval of 6 nm (~1.6 THz) in the near-infrared is accomplished by the photoexcitation at 532 nm of a surface photonic crystal having an overlayer (superstrate) of optically-active azobenzene polymer. Optical excitation of an azobenzene film drives the *trans*→*cis* isomerization of the molecule, thereby altering the index of refraction of the overlayer and shifting the resonant wavelength of the tunable reflector [5]. For 260 mW of incident power, the superstrate refractive index and peak reflectivity wavelength for the reflector are shifted by −0.05 and −6.2 nm, respectively, from their quiescent (zero power) values. Owing to the absence of any mechanically-movable elements, the requirement for only one mirror, and the dual role played by one semiconductor optical amplifier (SOA) as both oscillator and amplifier in a MOPA configuration, the laser system reported here represents a departure from conventional tunable ring and external cavity lasers.

## 2. Design and fabrication of the photonic crystal reflector

Figure 1 is a cross-sectional diagram of the tunable resonant reflector at the heart of the laser system. Similar to the design introduced by Dobbs and Cunningham [5], this structure (known as a guided mode resonant filter (GMRF)) incorporates a one-dimensional photonic crystal fabricated in ultraviolet-curable polymer on a 250 μm thick polyethylene terephthalate (PET) substrate. For maximum reflectivity in the vicinity of 850 nm, the grating period (Λ) and step height are chosen to be 550 nm and 170 nm, respectively. Following the fabrication of the grating by a multistep process [6,7] based on the replication of a silicon master mold, a 120 nm thick film of $TiO_2$ (index of refraction $n$ = 2.35) is deposited over the entire grating. Tuning the wavelength of peak reflectivity of the GMRF is accomplished with a thin layer of an azobenzene-isopropyl alcohol solution applied to the surface of the photonic crystal. The specific azobenzene dye adopted for these experiments is N-ethyl-N-(2-hydroxyethyl)-4-(4-nitrophenylazo) aniline [also known as Disperse Red 1 or DR1] and the thickness of the azobenzene-alcohol solution in Fig. 1 is estimated to be 5-10 μm. Fabrication of the reflector is completed by sealing the superstrate (azobenzene-alcohol solution) with a glass window ($n$ = 1.52). Figure 2 is a photograph of an array of the replica-molded gratings, prior to mounting each in a glass fixture and applying the azobenzene layer.

#158009 - $15.00 USD Received 21 Nov 2011; revised 1 Feb 2012; accepted 5 Jun 2012; published 12 Jun 2012

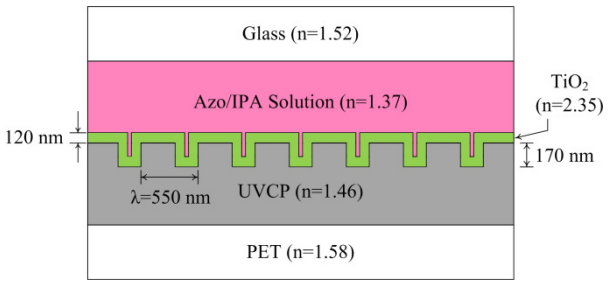


Fig. 1. Diagram in cross-section (not to scale) of the photonic crystal reflectance filter. The acronyms PET, UVCP, and Azo/IPA denote polyethylene terephthalate, ultraviolet-cured polymer, and the azobenzene-isopropyl alcohol solution, respectively. The index of refraction ($n$) for each component of the reflector is also indicated.

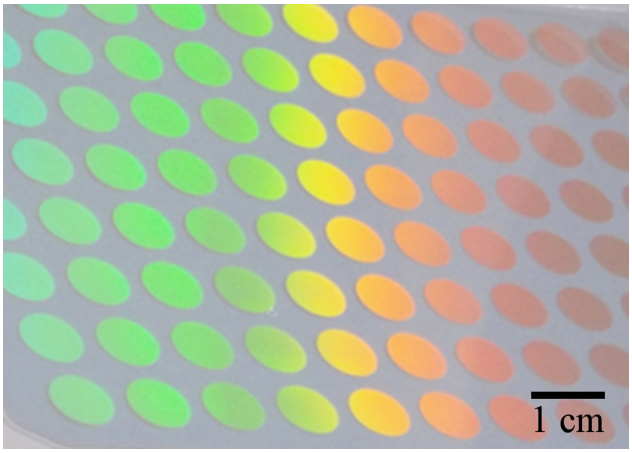


Fig. 2. An array of replica-molded gratings, photographed prior to mounting and the application of the azobenzene-alcohol solution.

Tuning of the wavelength of peak reflectivity for the resonant reflector occurs when the superstrate is illuminated by an external optical source of the proper wavelength. Doing so alters the index of refraction of the azobenzene/IPA solution owing to *trans*→*cis* isomerization transitions of the molecule. The transformation of the azobenzene molecule from the extended and linear *trans* form to the bent conformation of the *cis* configuration has the effect of reducing the dielectric permittivity and the refractive index of the azobenzene solution [5]. Since the *trans*→*cis* transition entails the absorption of a single photon, the change in refractive index ($\Delta n$) of the superstrate layer is expected to vary linearly with the intensity of the external optical source. The variation in the refractive index of an azobenzene dye in response to an optical stimulus is the basis for a variety of optical switching and data storage devices [8,9].

For the structure of Fig. 1, the quiescent (zero illumination) refractive index of the azobenzene/IPA superstrate is 1.37 which (as will be evident in Fig. 6) yields a resonant wavelength for the reflector of ~848.6 nm. As illustrated by Fig. 3, calculations of the dispersion relation for the photonic crystal resonant reflector (Fig. 1) do, indeed, predict a clear bandgap at normal incidence ($\sin^{-1} k_1/k_0 = 0$) and highest reflectivity (~80%) in the vicinity of 848 nm. Simulations of the spectral profile for the normalized reflectivity of the resonant filter are shown in Fig. 4 for several values of the superstrate refractive index in the $n$ = 1.0-1.43 interval. Note the rapid deterioration in the wavelength selectivity of the reflector (i.e., spectral width of the reflectivity profile) as the index of refraction falls to unity.

#158009 - $15.00 USD Received 21 Nov 2011; revised 1 Feb 2012; accepted 5 Jun 2012; published 12 Jun 2012

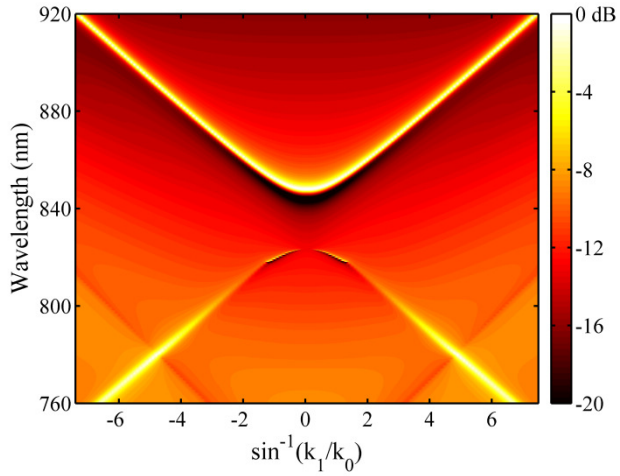


Fig. 3. Calculated dispersion diagram for the photonic crystal-based reflector of Fig. 1. To improve contrast, the maximum suppression illustrated was limited to 20 dB.

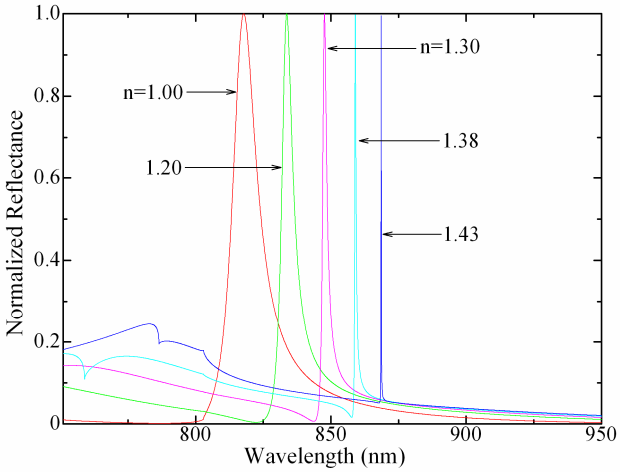


Fig. 4. Expected variation (with superstrate refractive index *n*) of the normalized reflectance profiles for the tunable filter of Fig. 1. Simulations are presented for 5 values of *n* ranging from 1.0 to 1.43.

## 3. Ring laser configuration

The component arrangement for the tunable ring laser is presented in Fig. 5. Throughout these experiments, the reflector was illuminated (at 30° with respect to the surface normal) and tuned with the frequency-doubled output of a cw Nd:$YVO_4$ laser. Although 532 nm lies ~40 nm to the red of peak absorption for the DR1/IPA solution ($\lambda_{max}$ ~492 nm) [5], measurements show that irradiation at this wavelength tunes the reflector toward the blue in a linear manner at the rate of 0.024 nm per mW of incident power. For the maximum available Nd:$YVO_4$ laser power of 260 mW, the superstrate refractive index is reduced by $5 \times 10^{-2}$ which corresponds to a blueshift>6 nm in the resonant wavelength of the reflector.

Gain for the laser of Fig. 5 is provided solely by a semiconductor optical amplifier having anti-reflection coatings ($R = 10^{-3}$) on both facets and producing a gain spectrum with a maximum at ~843 nm and a width (FWHM) of nominally 14-15 nm. Amplified spontaneous emission emerging from one end of the amplifier is transmitted by an isolator (which enforces

#158009 - $15.00 USD Received 21 Nov 2011; revised 1 Feb 2012; accepted 5 Jun 2012; published 12 Jun 2012

unidirectionality of the ring laser) and enters a coupler. Approximately 50% of the power incident on the coupler is delivered to an external fiber arm containing a polarization controller (Thorlabs FPC 020) which aligns the polarization of the photons so as to be perpendicular to the orientation of the grating in the photonic crystal reflector. (For the configuration of Fig. 5, no polarization maintaining fiber is required). A collimator directs the resulting TM-polarized optical field onto the reflector at normal incidence. Optical radiation back-reflected from the resonant filter is redirected to the SOA (via port 2) but this "narrow banded" portion of the original ASE spectrum enters the amplifier from the right. The output spectrum and power of the laser are monitored through port 4 of the coupler. For spectral measurements, single mode fiber having a core diameter of 11 μm connects the coupler port to an Ando spectrometer having a resolution (in first order) of 50 pm. In summary, the essence of the laser system of Fig. 5 is the continuous amplification by the SOA of optical radiation whose spectral distribution is selected by the photonic crystal reflector.

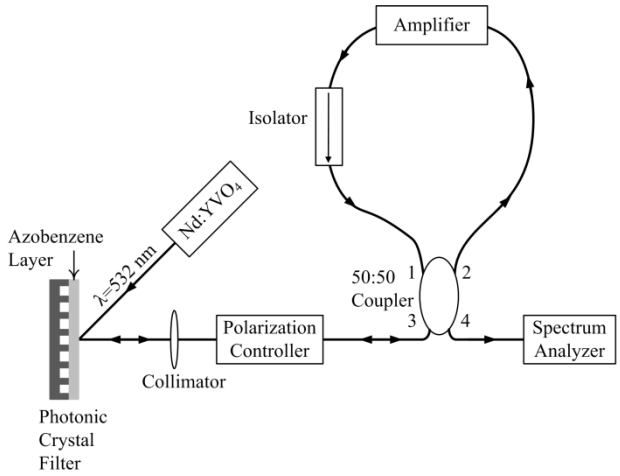


Fig. 5. Configuration of the tunable laser ring in which a photonic crystal reflector is controlled by the 532 nm radiation produced by a frequency-doubled Nd:$YVO_4$ laser.

## 4. Results and discussion

Figure 6 is a superposition of three spectra, recorded in the ~833 to 862 nm wavelength interval, that illustrate several aspects of the laser system. When the SOA is detached from the system of Fig. 5 and operated with a current of 190 mA, the spectrum shown in blue is observed. Peak gain for this amplifier lies near 841 nm and the breadth (FWHM) of the spectral profile is ~15 nm. The measured reflectivity of the photonic crystal mirror, represented by the green curve in Fig. 6, exhibits a resonance (maximum reflectivity) at 848.6 nm when the 532 nm power ($P_{ext}$) directed onto the mirror is zero. The 3 dB bandwidth of the primary peak in the reflectivity profile is 1.84 nm and the skewing of the mirror response toward longer wavelengths is in agreement with theory (cf. Fig. 4). The ripples superimposed onto the reflector's spectrum have a periodicity of ~1 nm which is attributable to the low finesse Fabry-Perot cavity embodied by the 0.25 mm thick PET substrate for the reflector. With the full laser system in operation (red curve, Fig. 6) and $P_{ext} = 0$, the output spectrum is centered on the peak reflectivity of the photonic crystal mirror but its linewidth is < 0.4 nm. Consequently, despite operating the ring laser in the red wing of the SOA emission spectrum, the amplifier gain at this point is sufficient to collapse the laser linewidth (relative to the mirror resonance width) by at least a factor of four while suppressing slightly the ASE background. Measurements of the dependence of the laser output power on the SOA current are summarized in Fig. 7. Obtained under the same conditions ($P_{ext} = 0$) as those for the red

#158009 - $15.00 USD Received 21 Nov 2011; revised 1 Feb 2012; accepted 5 Jun 2012; published 12 Jun 2012

trace of Fig. 6, these data show the influence of ASE for currents as low as I = 140 mA but a sharp upturn in output power when the current exceeds190 mA.

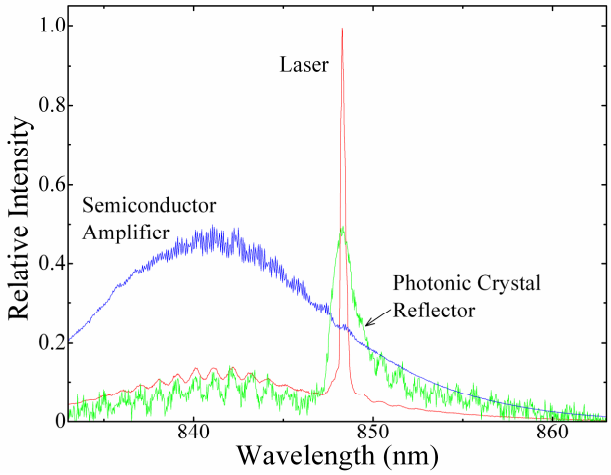


Fig. 6. Superposition of several spectra characteristic of the tunable ring laser: (blue) emission from the semiconductor amplifier (in isolation) for a drive current of 190 mA; (green) reflectance spectrum for the photonic crystal; (red) output of the ring laser. The latter two spectra were recorded when no 532 nm power (cf. Fig. 5) was directed onto the tunable reflector (i.e., $P_{ext} = 0$).

Figure 8 provides further contrast between the free-running SOA and the injection-seeded ring laser system. When an SOA is operated in the arrangement of Fig. 5 but with the photonic crystal reflector removed (as illustrated by the inset of Fig. 8), the spectrum shown in green is observed. In this configuration, lasing is facilitated by reflection from the now unterminated fiber at port 3 of the 50:50 coupler. Recorded for an SOA drive current of 120 mA, the free-running spectrum demonstrates that the longitudinal modes specified by the gain medium length become clearer than was evident in Fig. 6 (blue curve) and the strongest peaks are red-shifted with respect to the maximum of the SOA emission spectrum (cf. Fig. 6). In contrast, the injection-seeded laser system produces a single, narrow line at the wavelength dictated by the photonic crystal mirror ($\lambda_{inj}$).

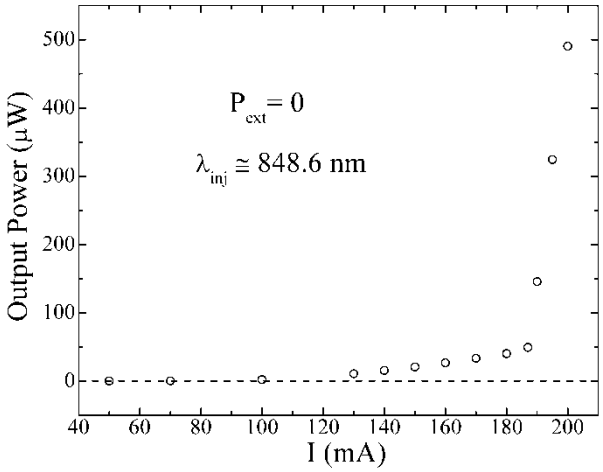


Fig. 7. Variation of the laser output power with SOA current when the GMRF (Fig. 1) is not illuminated ($P_{ext} = 0$).

#158009 - $15.00 USD Received 21 Nov 2011; revised 1 Feb 2012; accepted 5 Jun 2012; published 12 Jun 2012

Another demonstration of the impact of the GMRF on laser performance is provided by the laser spectra of Fig. 9. Specifically, these data were acquired with the photonic crystal reflector re-installed into the external arm of Fig. 5 but with the superstrate (azobenzene/IPA layer) removed from the reflector. In this situation, the spectrum narrows dramatically for SOA drive currents above ~120 mA and the longitudinal mode separation is determined by the thickness of the transparent PET substrate of the GMRF, in agreement with the reflectivity (green) spectrum of Fig. 6.

The performance of the ring laser as the tunable mirror is scanned ~6.2 nm to the blue of its quiescent ($P_{ext}$ = 0) position is summarized in Fig. 10. Throughout these experiments, the SOA drive current was fixed at 190 mA and, for convenience, all of the spectra are normalized. Furthermore, the data of Fig. 10(b) are identical to those of panel (a) of the figure but are illustrated in a semilog format. These data provide a vivid confirmation of the rapid line narrowing to be expected as the wavelength of peak GMRF reflectivity moves progressively closer to the region of peak gain. Specifically, as the optical power delivered to the reflector is raised to the maximum available value of 260 mW, the linewidth collapses to < 0.05 nm, the resolution limit of the spectrometer. Narrowing of the laser linewidth proceeds most rapidly when the wavelength of peak GMRF reflectivity falls below ~844 nm. This is the point at which the amplifier gain surpasses ~80% of its peak value and the rapid reduction in the output bandwidth is a well-known characteristic of high gain amplifiers that are injection-seeded [10,11]. In a similar manner, the efficiency for extracting power radiated by

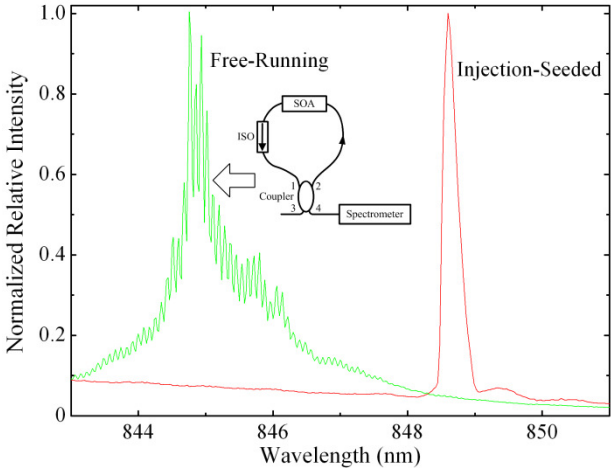


Fig. 8. Comparison of the normalized spectra generated by the free-running SOA (green) and the injection-seeded ring laser (red). In recording the free-running spectrum, the SOA current was fixed at 120 mA whereas, for injection-seeded operation, the current was maintained at 190 mA. The injection-seeded spectrum was recorded for $P_{ext}$ = 0. Also, the inset illustrates the experimental arrangement with which the free-running spectrum was acquired.

the semiconductor amplifier in a narrow line rises rapidly as the injection wavelength (resonant wavelength of the reflector) approaches 842 nm. It is evident from Fig. 10 that the broadband ASE background is suppressed to some degree at all injection wavelengths ($\lambda_{inj}$) studied but the magnitude of the effect rises precipitously for $\lambda_{inj} \leq 846$ nm. Peak ASE intensity for the $P_{ext}$ = 200 mW spectrum ($\lambda_{inj} \approx 844$ nm), for example, is suppressed by more than 16 dB relative to that for the $P_{ext}$ = 0 spectrum. In contrast, the dominant contribution to the laser's output power is provided by the ASE continuum when the peak reflectivity of the GMRF lies at $\lambda_{inj} \geq 846$ nm. This trend is underscored by the data of Fig. 11 which represent the calculated extraction efficiency of the ring laser for injection wavelengths between ~848.6 and 842.5 nm. The data indicate that, although extraction efficiencies above 97% are realized for $\lambda_{inj}$ = 842.5 nm, the fastest rise in efficiency occurs as $\lambda_{inj}$ decreases from ~847.5 nm to

#158009 - $15.00 USD Received 21 Nov 2011; revised 1 Feb 2012; accepted 5 Jun 2012; published 12 Jun 2012

846 nm – a span of only 1.5 nm. One concludes that extraction efficiency is impacted strongly by injection wavelengths almost 5 nm to the long wavelength side of peak gain whereas significant reductions in laser linewidth are not evident until injection seeding approaches within ~2 nm of the wavelength at which maximum gain occurs.

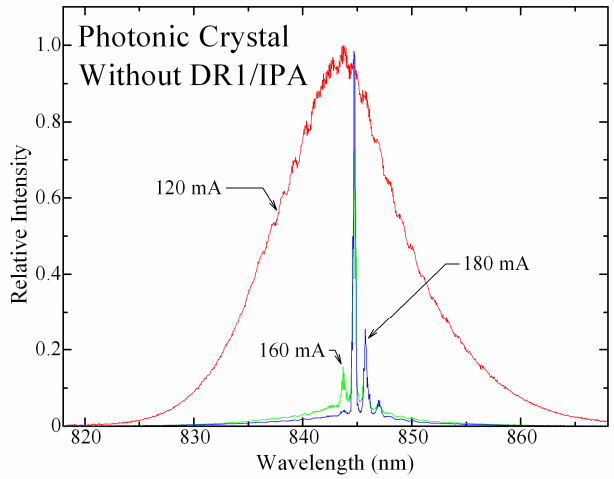


Fig. 9. Laser spectra recorded for three values of the SOA current (120 mA [red], 160 mA [green], and 180 mA [blue]) when the reflector of Fig. 1 has no superstrate (azobenzene/isopropyl alcohol) layer. The mode spacing in all of the spectra is attributable to the thickness of the reflector's PET substrate. For the sake of comparison of the three spectra, the 160 mA and 180 mA spectra have been attenuated.

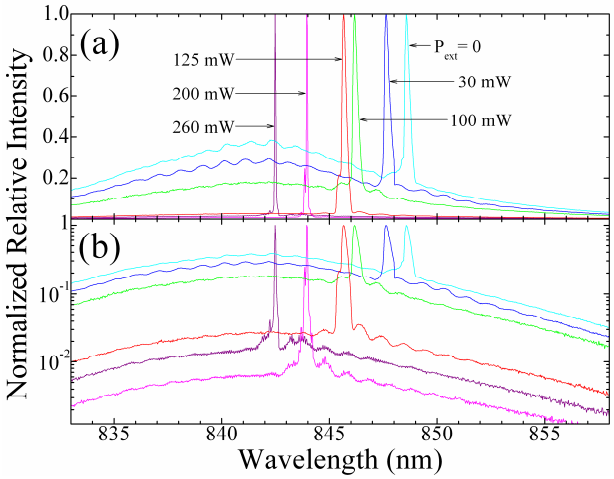


Fig. 10. (a) Superposition of six laser output spectra, each recorded with the reflector centered at a different wavelength. The green (532 nm) laser power $P_{ext}$ driving the tunable filter is indicated for each spectrum. All of the data were acquired with the SOA driving current maintained at 190 mA; (b) Same data as those of panel (a) but presented with the ordinate having a logarithmic scale.

#158009 - $15.00 USD Received 21 Nov 2011; revised 1 Feb 2012; accepted 5 Jun 2012; published 12 Jun 2012

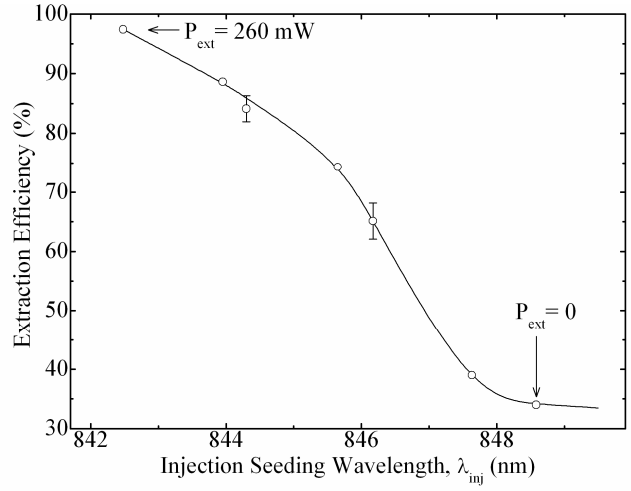


Fig. 11. Dependence of the laser extraction efficiency on the resonant wavelength of the tunable reflector (the injection wavelength, $\lambda_{inj}$) and, hence, the laser output. Representative estimated uncertainties (one standard deviation) are indicated for several of the measurements and the curve drawn through the data is intended only as a guide to the eye. Note that zero for the ordinate at left has been suppressed. In all of the experiments conducted to date, the amplifier extraction efficiency exceeded 33% and values above 97% were observed.

The data of Figs. 10 and 11 corroborate the presumption that the laser system reported here is one that is internally injection-seeded. Although configured in the form of a ring, this system behaves as an amplifier seeded by radiation selected by the photonic crystal reflector. In particular, the dominance of ASE in the laser output spectrum when the GMRF peak reflectivity is tuned beyond 846 nm demonstrates that the system does not function in this spectral region as a conventional ring laser. As much as 2/3 of the total power is emitted in a ~13 nm FWHM continuum and the power injected into the SOA from the GMRF is insufficient to significantly suppress the ASE. Rather than behaving as a ring, the laser of Fig. 5 resembles a class of laser systems often described as ASE, superradiant, or mirrorless lasers [12, 13]. Amplifiers with sufficient single pass gain are capable of producing output beams of high spatial quality ($M^2 < 2$) while dispensing with the conventional optical resonator and its attendant drawbacks such as sensitivity to misalignment and mechanical perturbations [12].

When $\lambda_{inj}$ falls below ~844 nm, however, the linewidth falls by at least a factor of 3 and the power stored under the SOA gain profile (power that, for $\lambda_{inj} > 846$ nm, is radiated almost entirely as broadband ASE) is efficiently extracted in a narrow line. Similar behavior has been observed previously when injection seeding other broadband, high gain amplifiers such as the KrF (248 nm) [14], metal-halide (CdI: 655 nm, HgBr:502 nm) [15], and dye laser systems. These conclusions are underscored by Fig. 12 which presents spectra corresponding to those of Fig. 6 when the wavelength for maximum reflectivity of the photonic crystal is 843.9 nm because $P_{ext}$ = 200 mW. It is clear that the ASE background has essentially vanished and the linewidth of the output is considerably narrower than its counterpart in Fig. 6. It can be concluded that, when $842.5 \leq \lambda_{inj} \leq 846$ nm, the SOA of Fig. 5 serves a dual function as both the oscillator and amplifier in an internally-seeded MOPA system and the system conforms to the behavior of a conventional ring laser. A critical role is played by the photonic crystal reflector which selects only a portion of the original ASE spectrum and directs the spectral slice to the far end of the SOA. In effect, the tunable reflector injection seeds the amplifier, a function that is generally reserved in MOPA systems for an entirely separate stage or unit [10].

#158009 - $15.00 USD Received 21 Nov 2011; revised 1 Feb 2012; accepted 5 Jun 2012; published 12 Jun 2012

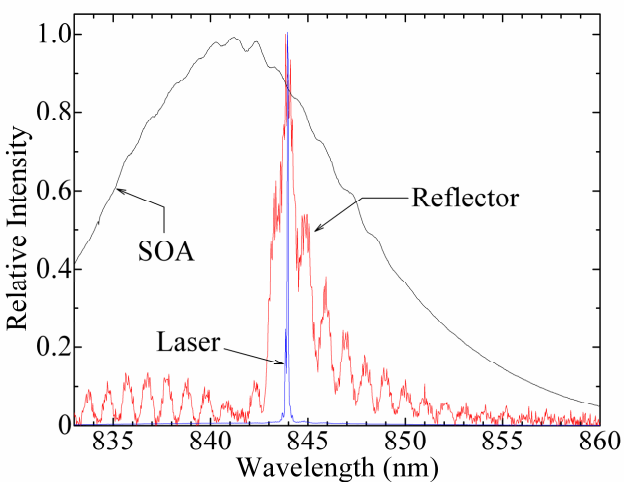


Fig. 12. Spectra analogous to those of Fig. 6 but for which the peak reflectivity of the photonic crystal mirror lies at 843.9 nm. The SOA current is again fixed at 190 mA.

## 6. Summary and conclusions

The design and performance of a ring laser, injection-seeded internally, have been described. Based on an SOA which essentially serves simultaneously as both the master oscillator and amplifier in a MOPA configuration, this laser relies on an optically-tuned photonic crystal reflector to filter the ASE generated by the SOA and re-inject it into the ring. Spectral narrowing of the laser linewidth owing to the high gain amplifier is striking when the central injection wavelength provided by the tunable reflector approaches within ~2 nm of the wavelength for peak gain in the SOA. Surprisingly, the efficiency for extracting, in a narrow line, power radiated by the amplifier is favorably impacted by injection wavelengths almost 5 nm to the red of peak gain.

A prominent feature of the laser system reported here is its simplicity and, in particular, the elimination of the external injection seeder that is required in conventional MOPA systems. Because the SOA, in tandem with the photonic crystal reflector, provides its own seed radiation, the system is both compact and inexpensive. Perhaps of greater import is the potential of this laser design as a subsystem in a fully-optical system in which one laser driver is able to tune the frequencies of multiple, remotely-located oscillators.

## Acknowledgments

The expert technical assistance of V. Mowery and C. Coxsey as well as the support of this work by the U. S. Air Force Office of Scientific Research (H. R. Schlossberg) under grant no. FA9550-10-1-0456 are gratefully acknowledged. J. Zheng and C. Ge contributed equally to this work.

#158009 - $15.00 USD Received 21 Nov 2011; revised 1 Feb 2012; accepted 5 Jun 2012; published 12 Jun 2012